

SOURCE  
DATATRANSPARENT  
PROCESSOPEN  
ACCESS

# Peroxisomal protein PEX13 functions in selective autophagy

Ming Y Lee<sup>1</sup>, Rhea Sumpter Jr<sup>1</sup>, Zhongju Zou<sup>1,2</sup>, Shyam Sirasanagandla<sup>1</sup>, Yongjie Wei<sup>1,2</sup>, Prashant Mishra<sup>3</sup>, Hendrik Rosewich<sup>4</sup>, Denis I Crane<sup>5</sup> & Beth Levine<sup>1,2,6,\*</sup>

## Abstract

PEX13 is an integral membrane protein on the peroxisome that regulates peroxisomal matrix protein import during peroxisome biogenesis. Mutations in PEX13 and other peroxin proteins are associated with Zellweger syndrome spectrum (ZSS) disorders, a subtype of peroxisome biogenesis disorder characterized by prominent neurological, hepatic, and renal abnormalities leading to neonatal death. The lack of functional peroxisomes in ZSS patients is widely accepted as the underlying cause of disease; however, our understanding of disease pathogenesis is still incomplete. Here, we demonstrate that PEX13 is required for selective autophagy of Sindbis virus (virophagy) and of damaged mitochondria (mitophagy) and that disease-associated PEX13 mutants I326T and W313G are defective in mitophagy. The mitophagy function of PEX13 is shared with another peroxin family member PEX3, but not with two other peroxins, PEX14 and PEX19, which are required for general autophagy. Together, our results demonstrate that PEX13 is required for selective autophagy, and suggest that dysregulation of PEX13-mediated mitophagy may contribute to ZSS pathogenesis.

**Keywords** autophagy; mitophagy; PEX13; virophagy; Zellweger syndrome

**Subject Categories** Autophagy & Cell Death; Membrane & Intracellular Transport; Microbiology, Virology & Host Pathogen Interaction

**DOI** 10.15252/embr.201642443 | Received 26 March 2016 | Revised 4 October 2016 | Accepted 7 October 2016 | Published online 8 November 2016

**EMBO Reports (2017) 18: 48–60**

## Introduction

Fourteen human *PEX* genes have been characterized thus far, encoding peroxin proteins that function in various stages of peroxisome biogenesis, including membrane formation, import of peroxisomal matrix proteins, and peroxisome proliferation [1,2]. Peroxisomal membrane proteins have also been implicated as signaling platforms involved in reactive oxygen species (ROS)-induced autophagy [3]

and antiviral immunity [4]. Similar to other *PEX* genes, *PEX13* was originally identified and has been best studied in the context of its role in peroxisome biogenesis and ZSS [5,6]. Biochemically, many ZSS patients present with elevated levels of substrates normally processed by peroxisomes (e.g., very long-chain fatty acids) and reduced levels of products normally synthesized by peroxisome metabolism (e.g., plasmalogens) [7]. However, ZSS patients with normal peroxisome metabolite levels have been described, and the degree of peroxisomal metabolite abnormality does not always correlate with clinical severity [8–10]. The discrepancy in the biochemical and clinical phenotypes of ZSS patients suggests that at least a subset of *PEX* mutations may contribute to ZSS disease pathogenesis via additional molecular mechanisms independently of their role in peroxisome biogenesis.

Autophagy is a highly conserved pathway in eukaryotes characterized by the formation of double-membraned structures which deliver cytoplasmic contents to the lysosome for degradation [11,12]. In contrast to general autophagy, which nonselectively degrades cytoplasmic material to supply the cell with nutrients during starvation, selective autophagy functions during nutrient-rich conditions to remove specific harmful or unwanted structures. Diverse substrates have been described for selective autophagy, including protein aggregates (aggrephagy), mitochondria (mitophagy), peroxisomes (pexophagy), ribosomes (ribophagy), ER (reticulophagy), intracellular pathogens (xenophagy), and lipid droplets (lipophagy) [13,14]. Dysregulation of selective autophagy underlies numerous human pathologies, including neurodegeneration, infectious diseases, metabolic diseases, cancer, and aging, thus highlighting the important physiological roles of selective autophagy [11,15]. Cargo selectivity is determined by autophagic receptors; these receptors facilitate autophagosome engulfment of the cargo by interacting with both the cargo (which is commonly ubiquitylated) and LC3 family members on the autophagosomal membrane. Despite recent advances in characterizing several receptors such as p62, optineurin, and NBR1, our understanding of selective autophagy regulation remains limited [13]. Thus, we previously conducted a genome-wide siRNA screen to discover novel selective autophagy factors and

1 Center for Autophagy Research, Department of Internal Medicine, University of Texas Southwestern Medical Center, Dallas, TX, USA

2 Howard Hughes Medical Institute, University of Texas Southwestern Medical Center, Dallas, TX, USA

3 Children's Medical Center Research Institute at the University of Texas Southwestern Medical Center, Dallas, TX, USA

4 Department of Pediatrics and Pediatric Neurology, Georg August University, Göttingen, Germany

5 Eskitis Institute for Drug Discovery and School of Natural Sciences, Griffith University, Nathan, Qld, Australia

6 Department of Microbiology, University of Texas Southwestern Medical Center, Dallas, TX, USA

\*Corresponding author. Tel: +1 214 648 2202; E-mail: beth.levine@utsouthwestern.edu

identified PEX13 as a candidate selective virophagy and mitophagy factor [16].

## Results and Discussion

To evaluate whether *PEX13* is a *bona fide* selective virophagy factor, we examined the colocalization of mCherry-labeled capsid protein from Sindbis virus (SIN) and the autophagosomal marker GFP-LC3 in cells with normal or reduced PEX13 expression. SIN is a single-stranded RNA virus in the alphavirus family, and numerous previous studies have shown that SIN viral nucleocapsids are degraded by selective autophagy [16–18]. In HeLa cells stably expressing GFP-LC3 (HeLa/GFP-LC3 cells) and infected with SIN, four siRNA oligos that target *PEX13* (and decrease PEX13 expression [Fig 1A]) resulted in a decrease in colocalization between mCherry-capsid and GFP-LC3 puncta (Fig 1B and C). This decrease in colocalization was similar to that observed after knocking down *ATG7*, a core autophagy gene essential for autophagic vesicle elongation, and knocking down *SMURF1* [16] or *FANCC* [18], two previously described selective virophagy factors. The numbers of mCherry-capsid puncta and GFP-LC3 puncta were not decreased in PEX13-deficient, SMURF1-deficient, or FANCC-deficient cells (Fig EV1A and B), suggesting that the defect in colocalization is likely due to a block in targeting the substrate to the autophagosome rather than deficiencies in either viral replication or autophagosome formation. (The failure of knockdown of *ATG7*, a core autophagy protein, to block overall numbers of GFP-LC3 puncta but still decrease SIN capsid targeting to autophagosomes, is consistent with previous observations in the HeLa/V5 cells used in this study [17], which are a cell line specifically adapted to be more permissive for alphavirus growth). Importantly, to exclude the possibility that SIN was targeted to GFP-LC3 aggregates rather than true autophagosomes, we confirmed that PEX13 is required for colocalization between endogenous LC3 and mCherry-capsid (Fig EV1C–F).

We utilized murine embryonic fibroblasts (MEFs) derived from wild-type *Pex13* (*Pex13*<sup>+/+</sup>) and knockout *Pex13* (*Pex13*<sup>-/-</sup>) embryos to further confirm whether *Pex13* is required for SIN virophagy (Fig 1D and E). After infection with SIN expressing

mCherry-capsid and GFP-LC3, *Pex13*<sup>-/-</sup> MEFs showed a defect in the colocalization of mCherry-capsid with GFP-LC3, and no difference in the mCherry-capsid or GFP-LC3 puncta numbers (Figs 1E and EV1G and H). The defect in SIN virophagy in *Pex13*-deficient MEFs is not due to a defect in general autophagy, as three well-established assays to measure basal and starvation-induced flux, including Western blot detection of p62 degradation, Western blot detection of LC3-I to LC3-II conversion, and quantitation of GFP-LC3 puncta in the presence or absence of the lysosomal inhibitor, bafilomycin A1 (Baf A1), did not reveal any decreases in basal or starvation-induced autophagic flux in *Pex13*<sup>-/-</sup> MEFs (Fig 1F and G). Thus, taken together, our data indicate that *PEX13* is required for selective virophagy but not for general autophagy in mammalian cells.

To evaluate whether PEX13 is a mitophagy factor, we first compared the effects of *PEX13* and *ATG7* siRNA knockdown on Parkin-mediated mitophagy after treatment with the mitochondrial uncoupling agent carbonyl cyanide *m*-chlorophenyl hydrazine (CCCP) using HeLa cells stably transfected with Parkin (HeLa/Parkin cells) (Figs 2A and B, and EV2A). *PEX13* or *ATG7* knockdown did not affect basal mitochondrial morphology as assessed by immunofluorescence imaging of TOMM20, a mitochondrial outer membrane protein (Fig 2A). After CCCP treatment, the majority of Parkin-expressing cells treated with noncoding (NC) siRNA lacked TOMM20 signal, indicating clearance of damaged mitochondria (Fig 2A and B). In contrast, the clearance of damaged mitochondria was impaired after treatment with four different siRNAs targeted against *PEX13*; the level of impairment was similar to that observed after treatment with siRNA targeted against *ATG7*. At an early time point during mitophagy, we observed Parkin colocalization with TOMM20 even after *PEX13* knockdown, suggesting that Parkin recruitment to the mitochondria is similar in *PEX13*-deficient cells and control cells (Fig EV2B). We confirmed the role of *PEX13* in mitophagy using a combination of more selective inhibitors of mitochondrial respiration, oligomycin, and antimycin A (OA) (as CCCP may have direct effects on lysosomal function [19]) and by measuring the clearance of mitochondrial double-stranded DNA (mtDNA) (as the proteasomal system can contribute to the degradation of mitochondrial outer membrane proteins such as TOMM20 but not to mtDNA [20]). Our results indicate that four different siRNAs

### Figure 1. PEX13 is required for Sindbis virophagy but not general autophagy.

- A Western blot detection of PEX13, ATG7, SMURF1, and FANCC in HeLa/GFP-LC3 cells transfected with the indicated siRNA. Asterisk denotes nonspecific band.
- B Representative images of GFP-LC3 colocalization with mCherry-capsid at 10 h after Sindbis virus (strain AO30) infection of HeLa/GFP-LC3 cells treated with the indicated siRNA. siPEX13 oligo #2 is shown; similar results were observed with three other siPEX13 oligos. Arrowheads denote representative colocalized GFP-LC3/mCherry-capsid puncta. Scale bars, 10  $\mu$ m.
- C Quantification of colocalized GFP-LC3 and mCherry-capsid puncta normalized to the number of mCherry-capsid puncta per cell (% colocalization) in the experiment shown in (B). Bars are mean  $\pm$  SEM of triplicate samples (~100 cells analyzed per sample). Similar results were observed in more than three independent experiments. \*\*\* $P < 0.001$ ; one-way ANOVA with adjustment for multiple comparisons. See Fig EV1A and B for quantification of mCherry-capsid puncta per cell and GFP-LC3 puncta per cell from the same experiment.
- D Western blot detection of Pex13 in MEFs of indicated genotype. Asterisks denote nonspecific bands.
- E Quantification of colocalized GFP-LC3 and mCherry-capsid puncta normalized to the number of mCherry-capsid puncta per cell (% colocalization) at 8 h after Sindbis virus (AO28 strain) infection in MEFs of the indicated genotype. Bars are mean  $\pm$  SEM of triplicate samples (~100 cells analyzed per sample). Similar results were observed in more than three independent experiments. \* $P < 0.05$ ; two-tailed unpaired t-test. See Fig EV1G and H for quantification of mCherry-capsid puncta per cell and GFP-LC3 puncta per cell from the same experiment.
- F Western blot detection of p62 and LC3 in MEFs of indicated genotype treated with 100 nM Baf A1 or DMSO vehicle and cultured in normal medium (starvation “–”) or EBSS (starvation “+”) for 3 h. Similar results were observed in three independent experiments.
- G Quantification of GFP-LC3 puncta in MEFs of indicated genotype treated with 10 nM Baf A1 or DMSO vehicle and cultured in normal medium or HBSS (starvation “+”) for 3 h. Bars are mean  $\pm$  SEM of triplicate samples (~100 cells analyzed per sample). \* $P < 0.05$ ; two-tailed unpaired t-test. NC, nonsilencing control.

Source data are available online for this figure.

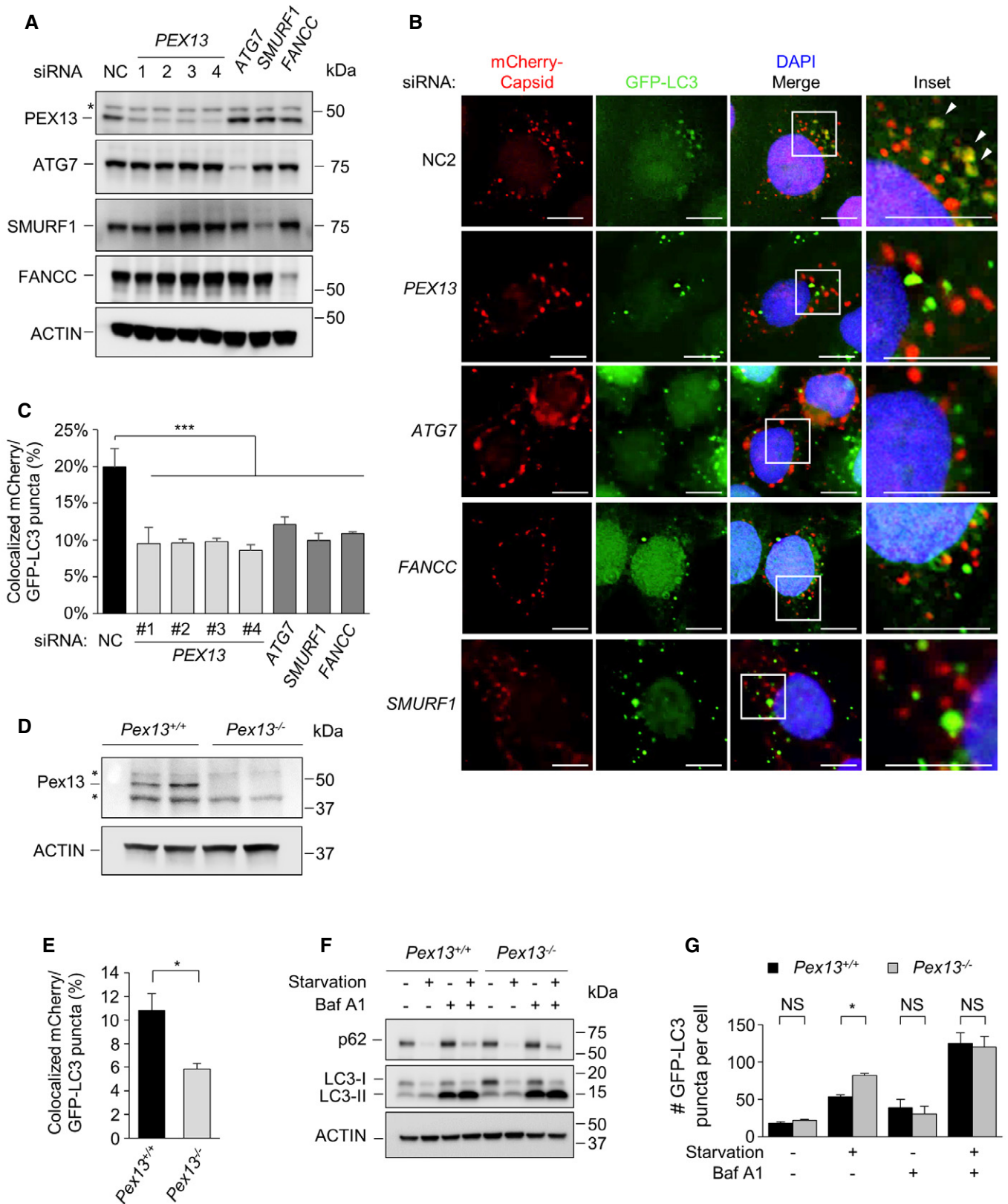


Figure 1.

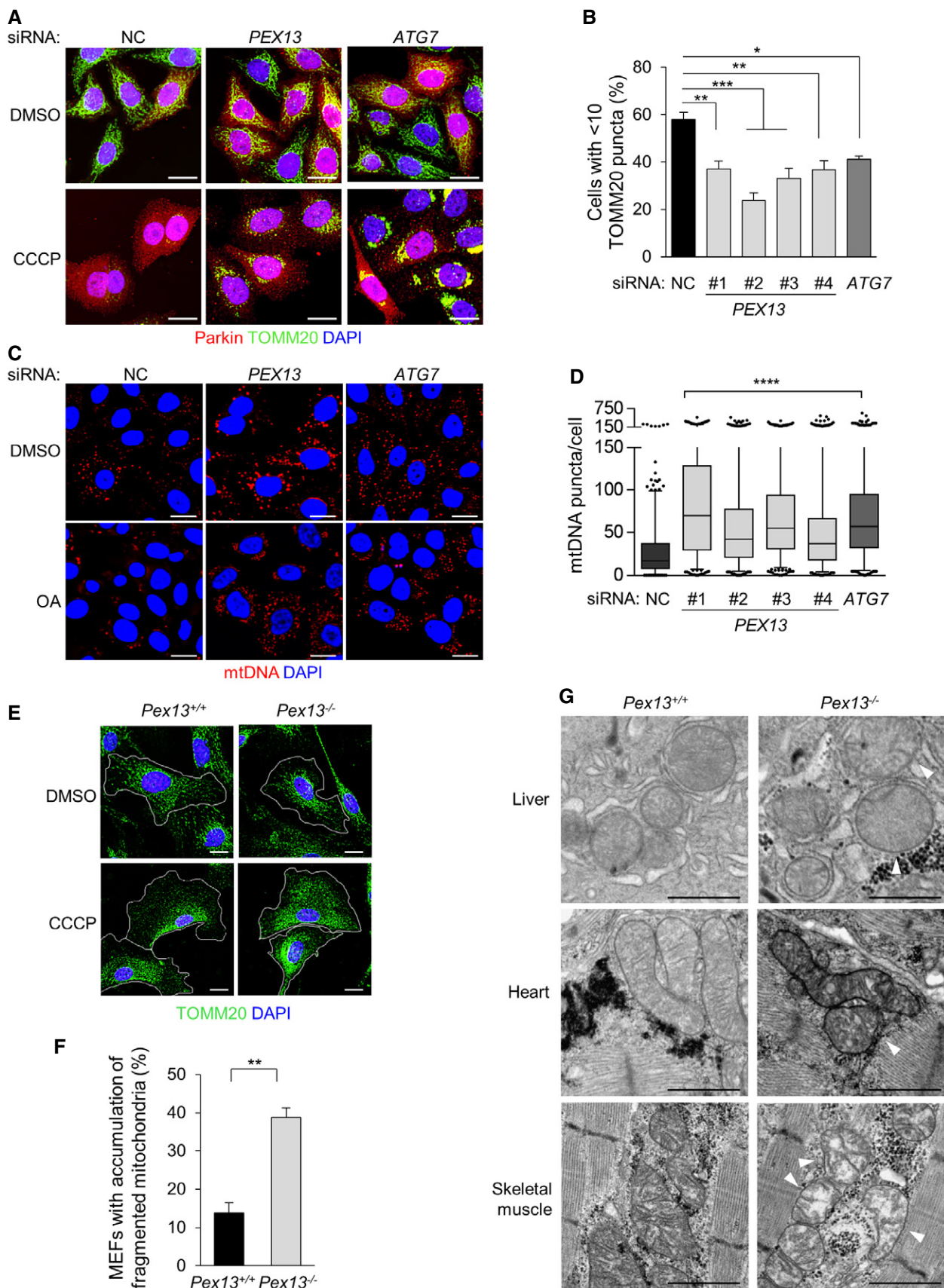


Figure 2.

**Figure 2. PEX13 is required for mitophagy.**

- A Representative images of Parkin-mediated clearance of mitochondrial outer membrane protein TOMM20 in HeLa/Parkin cells treated with indicated siRNA 16 h after treatment with 10  $\mu$ M CCCP or DMSO vehicle control. siPEX13 oligo #2 is shown; similar results were observed with three other siPEX13 oligos. Scale bars, 20  $\mu$ m.
- B Quantification of TOMM20 clearance in the experiment shown in (A). Results represent mean  $\pm$  SEM of triplicate samples (~100 cells analyzed per sample). Similar results were observed in more than three independent experiments. \* $P$  < 0.05, \*\* $P$  < 0.01, \*\*\* $P$  < 0.001; one-way ANOVA with adjustment for multiple comparisons.
- C Representative images of Parkin-mediated clearance of mitochondrial double-stranded DNA (mtDNA) in HeLa/HA-Parkin cells treated with indicated siRNA 8 h after treatment with 2.5  $\mu$ M oligomycin and 250 nM antimycin A (OA) or DMSO vehicle control. siPEX13 oligo #1 is shown; similar results were observed with three other siPEX13 oligos. Nuclear DNA staining was masked using DAPI. Scale bars, 20  $\mu$ m.
- D Quantification of mtDNA clearance in the experiment shown in (C). Results represent box plots of ~300 cells analyzed per sample. Whiskers represent 5–95% range and the horizontal lines of the boxes indicate the 25<sup>th</sup>, 50<sup>th</sup> and 75<sup>th</sup> percentiles of the dataset. Each outlier is represented by a dot. Similar results were observed in three independent experiments. \*\*\*\* $P$  < 0.0001; Kruskal–Wallis  $H$ -test.
- E Representative images of TOMM20 fragmentation or compaction around perinuclear region in MEFs of the indicated genotype 24 h after treatment with 30  $\mu$ M CCCP or DMSO vehicle control. White lines indicate cell borders. Scale bars, 20  $\mu$ m.
- F Quantification of percentage of cells in experiment shown in (E) with accumulation of fragmented mitochondria after CCCP treatment. Results represent mean  $\pm$  SEM of triplicate samples (~100 cells analyzed per sample). Similar results were observed in three independent experiments. \*\* $P$  < 0.01; two-tailed unpaired  $t$ -test.
- G Electron microscopic analysis of E18.5 mouse embryonic liver, heart, and skeletal muscle. Shown are representative images from one mouse. Similar results were observed in three mice per genotype. Arrowheads indicate damaged mitochondria. Scale bars, 1  $\mu$ m.

targeting PEX13 block OA-induced mtDNA clearance as effectively as ATG7 siRNA (Fig 2C and D).

Next, we evaluated mitochondrial morphology and function in *Pex13*<sup>+/+</sup> and *Pex13*<sup>-/-</sup> primary MEFs. During basal conditions, we observed similar reticular mitochondria morphology in *Pex13*<sup>+/+</sup> and *Pex13*<sup>-/-</sup> MEFs, as assessed by TOMM20 immunostaining (Fig 2E). However, we did observe abnormal mitochondria with disorganized cristae in basal conditions in *Pex13*<sup>-/-</sup> MEFs using electron microscopy (Fig EV2C). In MEFs, endogenous Parkin expression is negligible [20] and Parkin overexpression in primary MEFs does not promote the complete clearance of TOMM20 during CCCP or OA-induced mitophagy as it does in HeLa cells. Instead, damaged mitochondria in primary MEFs undergo Parkin-independent partial clearance and compaction around the perinuclear region [16]. After CCCP treatment, TOMM20 staining showed that damaged mitochondria were compacted around the perinuclear region and partially degraded in *Pex13*<sup>+/+</sup> MEFs, whereas damaged mitochondrial fragments accumulated diffusely throughout the cytoplasm in *Pex13*<sup>-/-</sup> MEFs (Figs 2E and F, and EV2D). Ultrastructurally, many autolysosomes containing mitochondria and only a few cytoplasmic damaged mitochondria were found in CCCP-treated wild-type MEFs (Fig EV2C), suggesting that damaged mitochondria were degraded via autophagy. In contrast, damaged mitochondria accumulated in CCCP-treated *Pex13*<sup>-/-</sup> MEFs (Fig EV2C). Of note, mitochondrial oxygen consumption and extracellular acidification rate were similar between *Pex13*<sup>+/+</sup> and *Pex13*<sup>-/-</sup> MEFs, suggesting that *Pex13*<sup>-/-</sup> MEFs have no major defect in mitochondrial biogenesis (Fig EV2E and F). Taken together, our data suggest that Pex13 facilitates removal of damaged mitochondria, even in primary fibroblasts that lack Parkin expression.

To evaluate whether Pex13 may function in mitophagy *in vivo*, we performed ultrastructural analysis of tissues from *Pex13*<sup>+/+</sup> and *Pex13*<sup>-/-</sup> mouse embryos (as *Pex13*<sup>-/-</sup> mice die neonatally). We found widespread abnormal mitochondrial cristae structures in *Pex13*<sup>-/-</sup> livers, hearts, and skeletal muscles (Fig 2G), consistent with a previous report [21]. Since autophagy is the only known pathway for degrading large cellular components such as organelles and protein aggregates and animals with tissue-specific knockout of core autophagy genes accumulate similar morphologically abnormal mitochondria [11], these observations are consistent with an important homeostatic role of Pex13-mediated mitophagy in regulating

mitochondria quality *in vivo*. However, we cannot rule out that the accumulation of abnormal mitochondria in *Pex13* knockout mice is due to factors other than defective mitophagy—either related to abnormal peroxisomal biogenesis or alterations in mitochondrial or proteasome functions which may contribute to mitochondrial quality control.

Our findings raised the possibility that patients with ZSS due to PEX13 mutations may have defects in selective autophagy. To test this hypothesis, we compared the effects of siRNA-resistant wild-type (WT) and disease-associated mutation-encoding PEX13 expression plasmids on the rescue of selective autophagy after PEX13 siRNA knockdown in HeLa/Parkin cells (Fig 3A–C). We focused on mitophagy rather than virophagy because HeLa cells and MEF cells are resistant to SIN infection after plasmid transfection. PEX13 I326T [22] and PEX13 W313G [23] are less stable than WT PEX13, but with higher concentration of plasmid transfection we observed similar levels of protein expression of WT and mutated PEX13 in HeLa/Parkin cells (Fig 3A). By immunofluorescence imaging, endogenous PEX13 was undetectable, but overexpressed WT and mutated PEX13 could both be detected (Fig 3B), and they colocalized with the peroxisomal marker PMP70 (Fig EV3A). siRNA-resistant WT PEX13, but neither disease-associated mutant, PEX13 I326T or PEX13 W313G, partially rescued the mitophagy defect in CCCP-treated HeLa/Parkin cells with PEX13 knockdown (Fig 3C). Surprisingly, cells expressing the PEX13 I326T or PEX13 W313G mutants showed a greater mitophagy defect compared with cells with empty vector control (Fig 3C) and mitochondria in mutant transfected cells appeared fragmented and aggregated even during basal conditions (Fig EV3B). These data suggest that PEX13 proteins containing disease-associated mutations are not only defective in mitophagy, they may also have a gain-of-function effect on interfering with basal mitochondria quality control.

To more directly evaluate whether cells from patients with PEX13 ZSS disease-associated mutants have defects in mitochondrial clearance, we performed studies on primary fibroblasts derived from a patient with a PEX13 W313G homozygous mutation [23]. Like MEFs, primary human fibroblasts do not express endogenous Parkin and CCCP or OA treatment results in Parkin-independent partial mitochondrial clearance and compaction around the perinuclear region [18]. Similar to our findings in CCCP-treated *Pex13*<sup>-/-</sup> vs. *Pex13*<sup>+/+</sup> MEFs, OA treatment resulted in partial mitochondrial

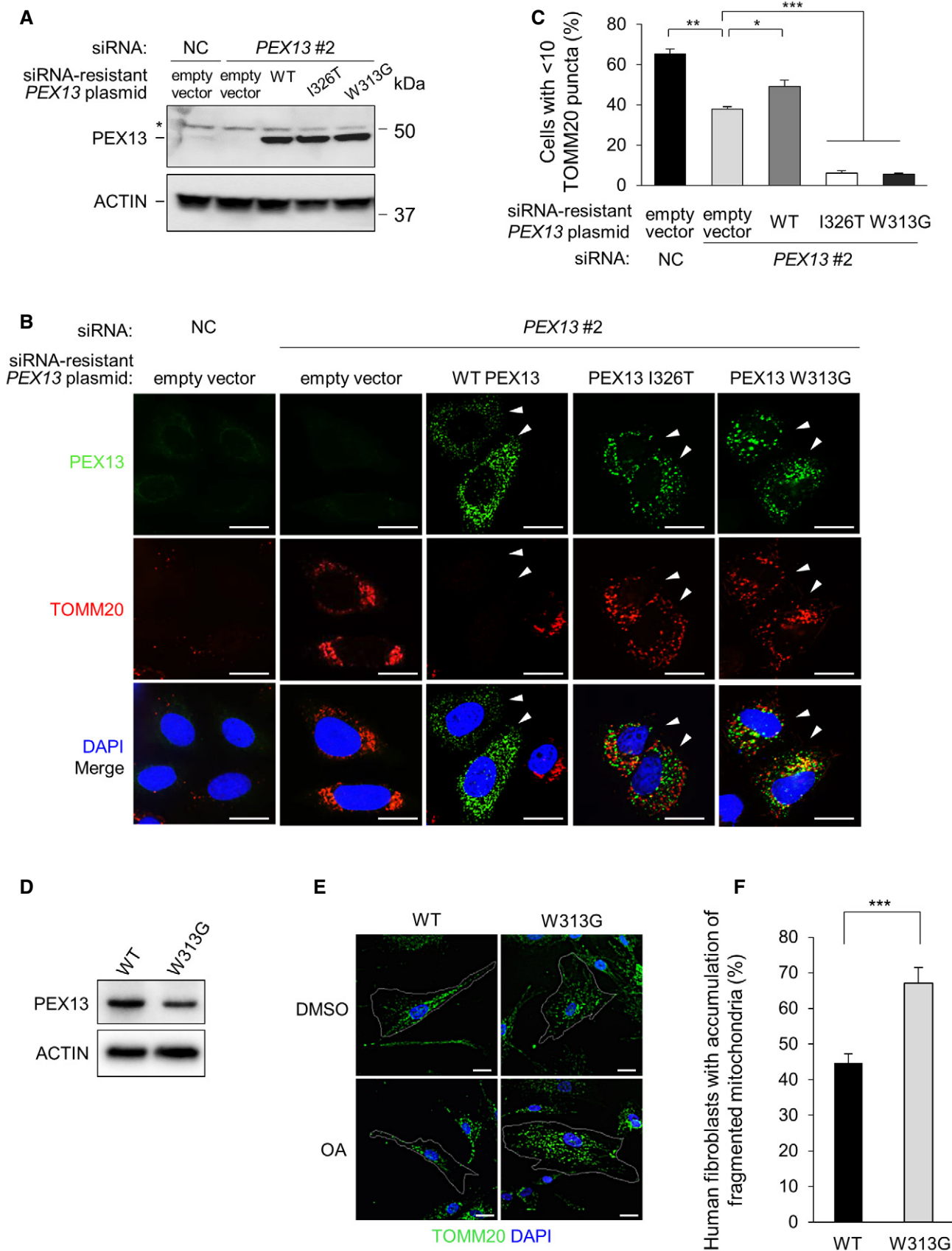


Figure 3.

**Figure 3. siRNA-resistant WT PEX13, but not disease-associated mutants PEX13 I326T and W313G rescue the mitophagy defect in PEX13 knockdown cells.**

- A Western blot detection of PEX13 in HeLa/Parkin cells transfected with indicated siRNA and siRNA-resistant *PEX13* plasmid. To achieve similar PEX13 protein expression levels, 0.75  $\mu$ g *PEX13* I326T and *PEX13* W313G plasmids were transfected compared with 0.25  $\mu$ g WT *PEX13*. Total plasmid level was adjusted using empty vector. Asterisk denotes nonspecific band.
- B Representative images of Parkin-mediated clearance of TOMM20 in HeLa/Parkin cells treated with *PEX13* siRNA and transfected with indicated *PEX13* siRNA-resistant plasmid and then treated with CCCP (10  $\mu$ M, 16 h). Arrowheads indicate cells expressing exogenous PEX13. Scale bars, 20  $\mu$ m. See Fig EV3B for representative images of mitochondrial morphology (TOMM20 staining) in control cells treated with DMSO.
- C Quantification of experiment shown in (B). Results represent mean  $\pm$  SEM of triplicate samples (~100 cells analyzed per sample). Similar results were observed in three independent experiments. \* $P < 0.05$ , \*\* $P < 0.01$ , \*\*\* $P < 0.001$ ; two-tailed unpaired t-test.
- D Western blot detection of PEX13 expression in wild-type (WT) and *PEX13* W313G (W313G) mutant primary human fibroblasts.
- E Representative images of Parkin-mediated clearance of TOMM20 in wild-type (WT) and *PEX13* W313G (W313G) mutant primary human fibroblasts treated with oligomycin (2.5  $\mu$ M) + antimycin A (250 nM) for 24 h. Scale bars, 20  $\mu$ m. W313G cells varied in morphology; outlined cell in upper right panel shows a representative cell with larger size and abnormal mitochondrial morphology (see Fig EV3C for higher resolution imaging) and outlined cell in lower right panel shows a representative cell with accumulation of fragmented mitochondria that would be scored as positive in (F).
- F Quantification of experiment shown in (E). Results represent mean  $\pm$  SEM of five groups of 10 images of random fields of cells (> 350 cells analyzed per sample). Similar results were observed in two independent experiments. \*\*\* $P < 0.0001$ ; two-tailed unpaired t-test.

Source data are available online for this figure.

clearance and compaction of remaining mitochondria in the perinuclear region, whereas fragments of damaged mitochondria accumulated throughout the cytoplasm in a higher percentage of *PEX13* W313G mutant than *PEX13* wild-type cells (Fig 3E and F). In the absence of OA treatment, the morphology of *PEX13* W313G cells was variable, and some cells (see example, upper right, Fig 3E) were larger and had abnormal-appearing mitochondria compared with wild-type fibroblasts. To further examine whether the defect in OA-induced mitophagy in *PEX13* W313G mutant fibroblasts is associated with basal abnormalities in mitochondria, we performed super-resolution structured illumination microscopy of wild-type and *PEX13* W313G mutant fibroblasts labeled with MitoTracker CMXrosamine (Mitotracker Red), a dye sensitive to mitochondrial membrane potential (Fig EV3C). Similar to our observations in *PEX13* siRNA-treated HeLa cells expressing *PEX13* W313G, the reticular mitochondrial network was markedly disrupted in *PEX13* W313G mutant fibroblasts. In addition, we found that, compared with wild-type cells, in *PEX13* W313G cells the overall intensity of MitoTracker Red staining was decreased, indicating a decrease in mitochondrial membrane potential. Taken together, these findings provide further evidence supporting a defect in basal mitochondrial quality control in *PEX13* W313G-expressing cells.

Next, we sought to characterize the subcellular localization and expression levels of PEX13 during mitophagy. PEX13 formed punctate staining that strongly colocalized with PMP70 during both basal and mitophagy conditions (Fig 4A). Moreover, PEX13 did not colocalize with TOMM20 (Fig 4B) nor with WIPI2, a marker of early autophagosomes [24] (Fig 4C). Furthermore, we did not observe any difference in PEX13 protein levels during mitophagy (Fig 4D). Together, our data suggest that PEX13 remains localized to the peroxisomal membrane and is not degraded during mitophagy. Since PEX13 remains localized to the peroxisomal membrane and does not colocalize with either the selective autophagic cargo (the mitochondria) or the early autophagic membrane during mitophagy, it likely does not function as a direct adaptor during selective autophagy.

Our findings raised the question of whether all proteins involved in peroxisome biogenesis function in mitophagy or whether PEX13 proteins (and potentially certain other PEX proteins) have a function independent of peroxisome biogenesis in mitophagy. During peroxisome biogenesis, PEX13 interacts with PEX14 and PEX5 for

peroxisomal matrix protein import, whereas PEX3 and PEX19 function upstream in the formation of peroxisomal membrane [2]. Since the peroxisome biogenesis function of PEX13 depends on other peroxin family members, we evaluated whether other peroxins are required for mitophagy and general autophagy. Of note, *PEX5* and *PEX19* are involved in ROS-induced general autophagy [3], and we previously identified *PEX3* as a candidate selective autophagy factor [16]. Using pools of four siRNAs targeting each gene, we knocked down *PEX3*, *PEX5*, *PEX13*, *PEX14*, or *PEX19* in HeLa cells (Fig 5A). The siRNA pool did not knock down *PEX5* efficiently (data not shown); thus, it was excluded from our study.

si*PEX3* and si*PEX13* treatment inhibited CCCP-induced TOMM20 clearance (Fig 5B) and OA-induced mtDNA clearance in HeLa cells expressing Parkin (Fig 5C). Using four individual siRNAs targeting *PEX3*, we further confirmed that PEX3 is required for selective mitophagy (Fig EV4). Similar to knockdown of *PEX13* (Fig EV2B), siRNA targeting *PEX3* did not block Parkin localization to mitochondria during mitophagy (Fig EV4B). Somewhat surprisingly, CCCP-induced TOMM20 clearance and OA-induced mtDNA clearance levels were normal in si*PEX14* and si*PEX19* treated HeLa/Parkin cells (Fig 5B and C). (Since *PEX19* is required for general autophagy, we had expected a partial decrease in mitophagy after *PEX19* knockdown.) Based on these data, we conclude that a deficiency in *PEX3* or *PEX13* inhibits mitophagy, whereas a deficiency in *PEX14* or *PEX19* does not inhibit mitophagy.

After transient knockdown of *PEX* genes in HeLa/Parkin cells for 48 h, we did not observe changes in the number or morphology PMP70 puncta (Fig EV5A and B). This is not surprising, as mammalian peroxisomes typically have a half-life of approximately 2 days during basal conditions [25]. The peroxisomes and mitochondria in these cells did not colocalize during basal and mitophagy conditions, similar to what we observed in control siRNA-treated cells (Fig EV5A and B). Thus, short-term deficiency of *PEX13*, *PEX3*, *PEX14*, or *PEX19* does not result in peroxisomal disappearance and does not alter peroxisome and mitochondria subcellular localization. Moreover, peroxisomal ghosts (labeled by PMP70 staining) in *Pex13*<sup>-/-</sup> MEFs did not colocalize with mitochondria during basal or mitophagy conditions (Fig EV5C).

Next, we evaluated whether these peroxins are involved in basal and starvation-induced general autophagy. We found that GFP-LC3 puncta numbers were similar in HeLa/GFP-LC3 cells treated with

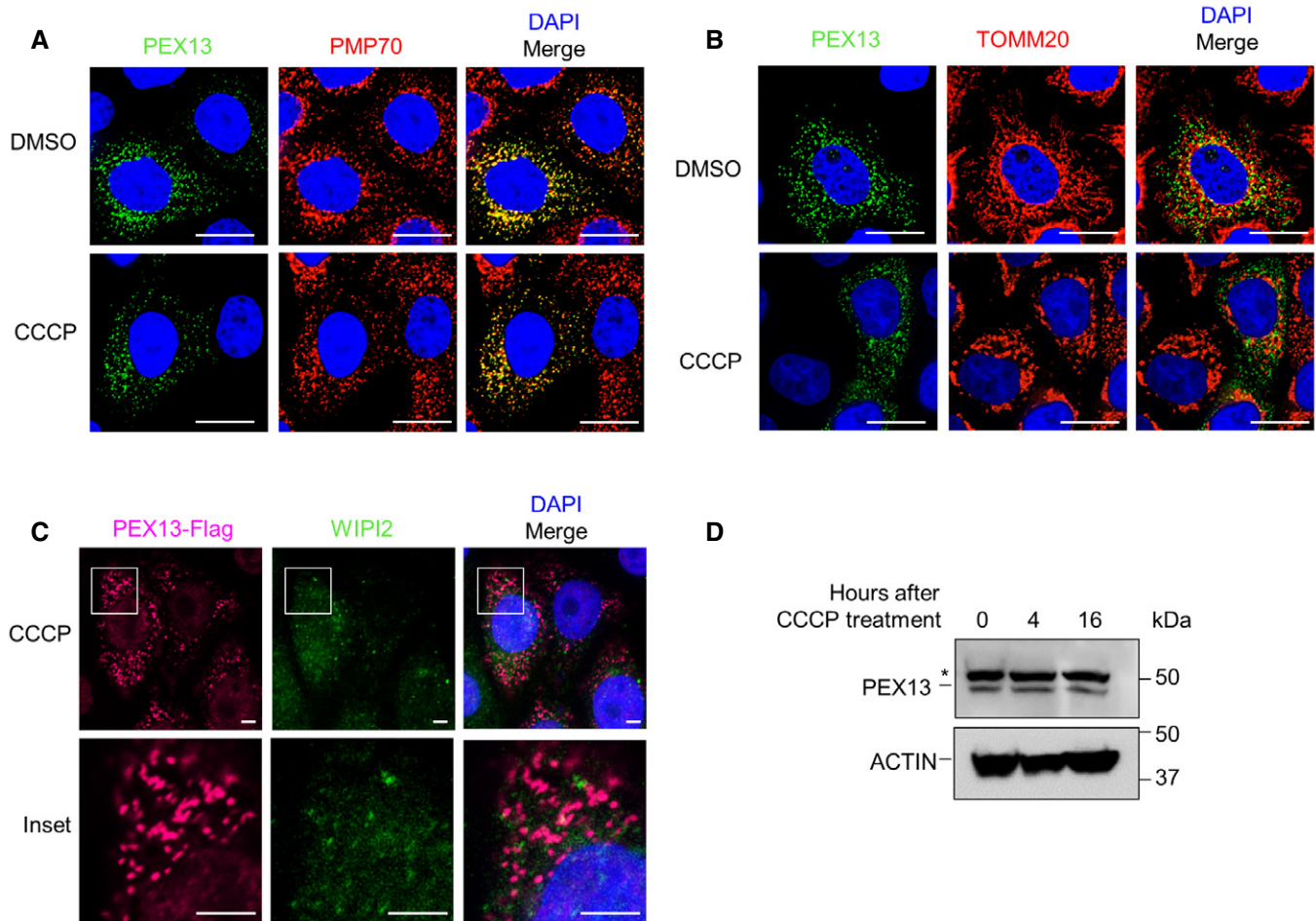


**Figure 4. PEX13 colocalizes with peroxisomes, but not with mitochondria or early autophagosomes during CCCP-induced mitophagy.**

A–C Representative images of PEX13 and PMP70 (A), PEX13 and TOMM20 (B), or PEX13-Flag and WIPI2 (C) colocalization in HeLa/Parkin cells transfected with PEX13 after 4 h DMSO or CCCP treatment.

D Western blot detection of endogenous PEX13 in HeLa/Parkin cells treated with 10  $\mu$ M CCCP for the indicated time. Asterisk denotes nonspecific band.

Data information: Scale bars, 20  $\mu$ m (A, B) and 5  $\mu$ m (C).

Source data are available online for this figure.

siPEX3, siPEX13, and control siRNA in basal and starvation conditions either in the presence or absence of Baf A1 treatment. In fact, PEX13 siRNA slightly increased autophagic flux in both conditions. Thus, neither PEX3 nor PEX13 are required for general autophagy. In contrast, PEX14 and PEX19 siRNA reduced GFP-LC3 puncta number during basal and starvation conditions to a similar extent as ATG7 siRNA, indicating reduced autophagic flux (Fig 5D). Similar autophagic flux analysis results were observed by quantifying endogenous LC3 puncta (Fig EV5D). These results corroborate a previous report indicating that PEX19 is required for general (ROS-induced) autophagy [3], and further identify starvation as an additional stimulus for PEX19-dependent autophagy pathway. In summary, we found that a subset of pexins, PEX13 and PEX3, are required for selective autophagy, whereas another subset of pexins, PEX14 and PEX19, are required for general autophagy.

In this study, we provide multiple lines of evidence supporting an essential role of PEX13 and PEX3 in selective, and not general,

autophagy in mammalian cells. Previous studies showed that PEX3 is required not only for peroxisome biogenesis, but also for peroxisomal degradation via pexophagy in yeast [26] and in mammalian cells [27]. Here, we showed that PEX13 is required for selective autophagy of two very different targets, a viral nucleocapsid protein and mitochondria, and that PEX3 is required for selective autophagy of mitochondria. Given that many factors involved in selective autophagy, including autophagy receptors (e.g., p62, NBR1, optineurin) and targeting signals (e.g., ubiquitin), mediate clearance of diverse substrates [13], we speculate that PEX3 and PEX13 may also be involved in other forms of selective autophagy.

Autophagy receptors facilitate the selective engulfment of cargo by the autophagosome by directly binding to the cargo and the autophagosomal membrane [13]. Our observation that PEX13 did not colocalize with markers of the early autophagosome (WIPI2) or with the selective autophagic cargo (TOMM20) during basal and

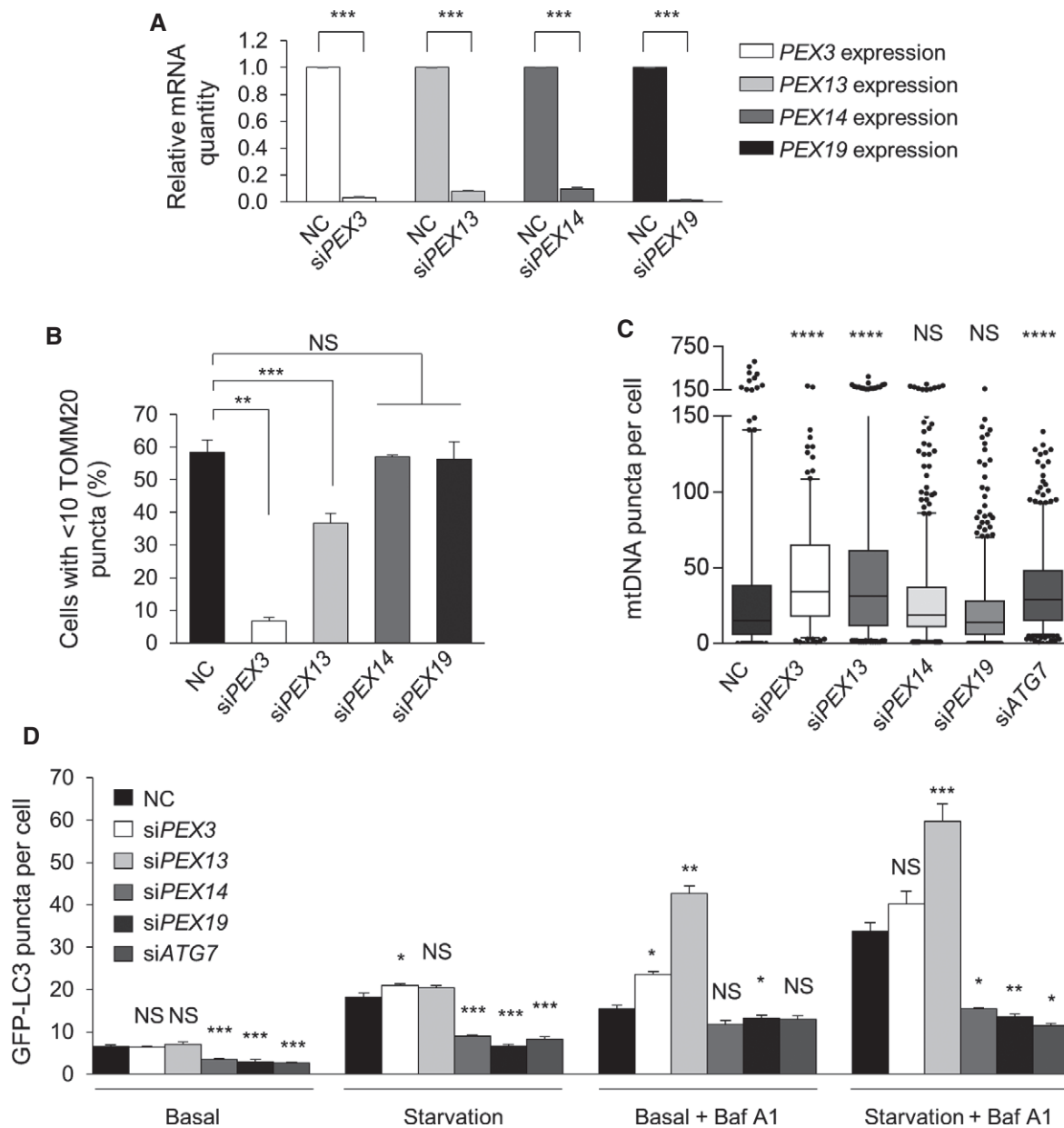


**Figure 5. PEX13 and PEX3 are required for selective mitophagy, whereas PEX14 and PEX19 are required for general autophagy.**

**A** Quantitative real-time PCR detection of mRNA levels for *PEX3*, *PEX13*, *PEX14*, and *PEX19* in HeLa cells transfected with the indicated siRNA. Results represent mean  $\pm$  SEM of triplicate samples. Similar results were observed in three independent experiments. \*\*\* $P < 0.001$ ; two-tailed unpaired *t*-test.

**B** Quantification of Parkin-mediated TOMM20 clearance in HeLa/Parkin cells transfected with the indicated siRNA 16 h after treatment with 10  $\mu$ M CCCP. Results represent mean  $\pm$  SEM of triplicate samples (~100 cells analyzed per sample). Similar results were observed in three independent experiments. \*\* $P < 0.01$ , \*\*\* $P < 0.001$ ; one-way ANOVA with adjustment for multiple comparisons.

**C** Quantification of mtDNA clearance in HeLa/HA-Parkin cells transfected with the indicated siRNA 8 h after treatment with 2.5  $\mu$ M oligomycin and 250 nM antimycin A (OA). Results represent box plots of ~300 cells analyzed per sample. Whiskers represent 5–95% range and the horizontal lines of the boxes indicate the 25<sup>th</sup>, 50<sup>th</sup>, and 75<sup>th</sup> percentiles of the dataset. Each outlier is represented by a dot. Similar results were observed in three independent experiments. \*\*\*\* $P < 0.0001$ , NS = not significant; Kruskal–Wallis *H*-test.

**D** Quantification of GFP-LC3 puncta in HeLa/GFP-LC3 cells treated with 10 nM Baf A1 or DMSO vehicle and cultured for 3 h in normal medium or HBSS starvation media. Results represent mean  $\pm$  SEM in triplicate samples (~100 cells analyzed per sample). Similar results were observed in three independent experiments. \* $P < 0.05$ , \*\* $P < 0.01$ , \*\*\* $P < 0.001$ , NS = not significant; one-way ANOVA with adjustment for multiple comparisons. Statistical analyses refer to the differences between *Pex* or *ATG7* siRNAs vs. NC siRNA within each treatment group.

mitophagy conditions suggests it does not function as an autophagy receptor. Given the precedent of peroxisome-associated proteins functioning as signaling platforms [3,4], we speculate that PEX13

may regulate selective autophagy as a peroxisomal membrane-associated signaling node, leading to downstream posttranslational modifications (such as ubiquitylation [28] or phosphorylation

[29,30]) and activation of other yet-to-be identified selective autophagy regulators. Unbiased proteomics approaches will be helpful to interrogate this pathway. From a teleological perspective, it is reasonable to postulate the dual function of certain proteins such as PEX13 in the biogenesis of peroxisomes—organelles that detoxify reactive oxygen intermediates—and in mitophagy, a process that involves the removal of damaged mitochondria that generate reactive oxygen intermediates.

Although the molecular mechanism underlying PEX13 regulation of selective autophagy remains to be determined, our study provides important insights into ZSS pathogenesis. Cells expressing the PEX13 disease-associated I326T and W313G mutant proteins showed a greater mitophagy defect compared with cells with PEX13 knockdown alone. Furthermore, overexpression of PEX13 with these mutations, but not wild-type PEX13, disrupted the normal reticular staining pattern of mitochondria during basal growth conditions. These results suggest that the disease-associated mutations interfere with mitophagy and mitochondrial quality control. In support of this hypothesis, mitochondria from patient fibroblasts homozygous for the W313G mutation had abnormal mitochondrial membrane potential and morphology during baseline conditions, and a defect in perinuclear mitochondrial compaction following treatment with a mitochondrial uncoupling reagent.

Abnormal mitochondria are frequently observed in patients with *PEX* mutations and have been suggested to contribute to ZSS disease pathogenesis [31,32]. The current prevailing paradigm is that mitochondrial dysfunction in ZSS is secondary to the defect in peroxisomal antioxidant functions and accumulation of lipid metabolites from the  $\beta$ -oxidation process [31]. Based on our discovery that a subset of *PEX* genes are required for selective autophagy (*PEX3* and *PEX13*), while another subset are required for general autophagy (*PEX14* and *PEX19*), we propose that dysregulation of mitochondrial quality control in cells with defective mitophagy or general autophagy contributes to ZSS pathogenesis. Defects in mitophagy-specific genes or core autophagy genes both lead to abnormal mitochondrial function, which contributes to the pathogenesis of aging, neurodegeneration, and cancer [33]. Our model is not mutually exclusive with the previous paradigm of ZSS pathogenesis; the two functions of *PEX13* could be additive in promoting mitochondrial health. Further studies are required to delineate the mechanisms by which peroxisome-associated proteins contribute to autophagy, as well as the role of autophagy defects in the pathogenesis of developmental disorders associated with mutations in peroxin proteins.

## Materials and Methods

### Cell culture

HeLa cells [34] (provided by V. Stollar) and HEK293T cells were cultured in DMEM containing 10% fetal bovine serum (FBS), 2 mM L-glutamine, and 1 $\times$  penicillin/streptomycin. HeLa/GFP-LC3 cells [17] were cultured in media containing 10  $\mu$ g/ml G418. HeLa/Parkin cells were generated by stable transfection of a pIRES-hyg3 vector (Clontech) expressing Parkin cDNA and cultured in media containing 100  $\mu$ g/ml hygromycin B. HeLa/

HA-Parkin cells were generated by retroviral transduction and cultured in media containing 0.25  $\mu$ g/ml puromycin (see “Retroviruses and lentiviruses” section for details). Primary murine embryonic fibroblasts (MEFs) were derived from day 13.5 embryos by crossing *Pex13*<sup>+/-</sup> mice and genotyped using previously described methods [21,35]. Additionally, mice that transgenically express GFP-LC3 [36] (provided by N. Mizushima) were crossed with *Pex13*<sup>+/-</sup> mice to obtain *Pex13*<sup>+/-</sup>/GFP-LC3 mice, and this strain was bred to harvest *Pex13*<sup>+/+</sup>/GFP-LC3 and *Pex13*<sup>-/-</sup>/GFP-LC3 MEFs. Primary MEFs were maintained in DMEM containing 15% FBS, 1 $\times$  penicillin/streptomycin, 120  $\mu$ M  $\beta$ -mercaptoethanol, and 1 $\times$  MEM nonessential amino acids and passaged no more than four times. Primary human fibroblasts from Zellweger syndrome patient fibroblast containing homozygous W313G mutation from control human subject without Zellweger syndrome were cultured in DMEM containing 10% FBS, 2 mM L-glutamine, and 1 $\times$  penicillin/streptomycin [23]. For starvation experiments, cells were cultured in Hank's balanced salt solution (HBSS) (Sigma, H9269) or Earle's balanced salt solution (EBSS) (Sigma, E7510) for the indicated time period. All cell lines were tested for mycoplasma contamination. HeLa cells and HeLa/Parkin cells were authenticated by STR profiling.

### Animal experiments

*Pex13*<sup>+/-</sup> and GFP-LC3 transgenic mice were housed and bred in a specific pathogen-free animal facility to obtain MEFs of the desired genotype and embryos for electron microscopic analyses. All animal experiments were approved by the UT Southwestern Institutional Animal Care and Use Committee.

### siRNA transfection

siRNA sequences and the source of siRNAs are provided in Appendix Table S1. siRNA was transfected using Lipofectamine 2000 (Invitrogen) or RNAiMAX (Invitrogen) at a final concentration of 50 nM according to the manufacturer's instructions 48 h before experiments.

### Sindbis virophagy assays

Recombinant Sindbis virus strains SIN-mCherry.capsid (strain AO30) and SIN-mCherry.capsid/GFP-LC3 (strain AO28) were generated, titered, and used for infections as previously described [16,37,38]. SIN-mCherry.capsid infections of HeLa/GFP-LC3 cells were performed at a multiplicity of infection (MOI) of five plaque-forming units (PFUs) per cell for 10 h. SIN-mCherry.capsid/GFP-LC3 infections of primary MEFs were performed at an MOI of 2.5 PFUs per cell for 16 h. Fluorescent microscopy images were analyzed by an observer blinded to experimental condition and the number of mCherry-capsid puncta, GFP-LC3 puncta, and colocalized mCherry-capsid/GFP-LC3 puncta was counted per cell.

### Mitophagy assays

HeLa/Parkin cells were treated with 10  $\mu$ M CCCP for 16 h, fixed, and then subjected to immunofluorescence staining to detect

TOMM20. The number of cells with < 10 mitochondria/cell and with  $\geq 10$  mitochondria/cell was counted by an observer blinded to experimental condition. For rescue experiments, HeLa/Parkin cells were treated with siRNA for 24 h, transfected with plasmids expressing siRNA-resistant WT or mutant PEX13 for an additional 24 h, and then treated with CCCP for 16 h. Additionally, HeLa/HA-Parkin cells were treated with 2.5  $\mu\text{M}$  oligomycin A and 250 nM antimycin A for 8 h, fixed, subjected to immunofluorescence staining to detect dsDNA, and analyzed by CellMask immunofluorescence imaging using Z-stacks (see “Immunofluorescence microscopy and image analysis” section for details). Primary MEFs and human fibroblasts were treated with 30  $\mu\text{M}$  CCCP or 2.5  $\mu\text{M}$  oligomycin A and 250 nM antimycin A, respectively, for 24 h, fixed, and then subjected to immunofluorescence staining to detect TOMM20. The number of cells with mitochondrial compaction around the nucleus and the number of cells with diffuse fragmentation of damaged mitochondria was counted by an observer blinded to experimental condition.

### Autophagy analyses

Autophagy was assessed by fluorescent microscopy quantification of GFP-LC3 puncta in *Pex13*<sup>+/+</sup>/GFP-LC3 MEFs, *Pex13*<sup>-/-</sup>/GFP-LC3 MEFs, and in HeLa/GFP-LC3 cells by an observed blinded to experimental condition as previously described [39] and by Western blot analysis of LC3. Autophagic flux was assessed by Western blot detection of p62 and LC3 and by quantitating GFP-LC3 puncta in the presence or absence of Baf A1. Autophagic flux was also assessed by quantitating endogenous LC3 puncta in the presence or absence of Baf A1.

### Immunofluorescence microscopy and image analysis

HeLa cells and MEFs were cultured on glass chamber slides (Lab-Tek), fixed in 2% paraformaldehyde (PFA) in PBS, permeabilized in 0.5% triton X-100/PBS, and then blocked with blocking buffer (0.5% BSA and 0.2% cold fish gelatin in PBS). Slides were incubated with primary antibodies overnight at 4°C, secondary antibodies at room temperature for 1 h, and then mounted with VectaShield containing DAPI (Vector). Negative control samples with only secondary antibody staining were used to determine background immunofluorescence levels. For experiments involving cellular segmentation, CellMask Deep Red (ThermoFisher C10046, 1:5,000) was applied with secondary antibodies. Z-stack images were acquired with a Zeiss AxioImager Z2 microscope equipped with a Photometrics CoolSnap HQ2 camera and a Zeiss PLAN APOCHROMAT 20 $\times$ /0.8 NA air objective or 63 $\times$ /1.3 NA oil objective using the same acquisition time for all samples within each experiment. Images were deconvolved using AutoDeBlur (Bitplane) and analyzed using the Cell module in Imaris version 8.2 (Bitplane). For images stained for double-stranded DNA related to quantitative image analysis of mitochondria DNA clearance, nuclear DNA staining was masked using Imaris by generating a nuclear surface using the DAPI channel and then setting non-DAPI signal within the nuclear surface to zero. For PMP70 and TOMM20 colocalization images, nonspecific nuclear staining was masked using Imaris. MEF and human fibroblast cell border outlines were drawn manually using Photoshop.

### Structured illumination microscopy of mitochondria

Cells were grown and treated with MitoTracker CMXRos on #1.5 coverslips in six-well plates. After treatment (50 nM, 30 min), cells were rinsed three times with complete medium, fixed in 2% PFA for 10 min, and rinsed with PBS. After fixation, coverslips were placed inverted onto ~50  $\mu\text{l}$  Prolong Diamond mounting medium (Invitrogen) on glass slides. Images were acquired with a Deltavision OMX SR microscope (GE) equipped with an Olympus PLAPON 60X/1.42 NA objective and channel-dedicated pco.edge sCMOS cameras (PCO). SIM reconstructions and 3D projections were performed using Deltavision softWoRx software (GE).

### Western blot analyses

Cultured cells were lysed in buffer containing 150 mM NaCl, 25 mM HEPES, 1 mM EDTA, 1% Triton X-100, protease inhibitor mixture (Roche Applied Sciences), and Halt phosphatase inhibitor cocktail (Thermo Scientific) for 1 h at 4°C, boiled in Laemmli buffer containing 2.5%  $\beta$ -mercaptoethanol for 5 min, separated by SDS-PAGE, and then transferred to PVDF membranes. Membranes were blocked in 5% milk for 1 h and then incubated in the indicated antibodies. Membranes were imaged using ECL Prime Western Blotting Detection Reagent (GE Healthcare) or Supersignal<sup>®</sup> West Pico Chemiluminescent Substrate kit (Pierce) on a digital imaging system (BioSpectrum, UVP).

### Quantitative real-time-PCR

Total RNA was isolated from cells using the RNeasy Plus Mini Kit (Qiagen) and 1  $\mu\text{g}$  RNA was used to generate cDNA (iScript, Bio-Rad). Quantitative RT-PCR was performed using the SYBR Green Master Mix (Qiagen) and detected using a 7500 Fast Real-Time PCR System (Applied Biosystems). Primers for the reactions are listed in Appendix Table S2.

### Electron microscopy

Tissue samples from day 18.5 mouse embryos and primary MEFs were treated with CCCP or DMSO vehicle, prepared for electron microscopy as described [40], and imaged using a JEOL 1200EX microscope equipped with an SIS Morada CCD camera.

### Mitochondrial functional assays

Oxygen consumption rate and proton production rate, as assessed by extracellular acidification rate, were assessed in a Seahorse Biosciences Extracellular Flux Analyzer (model XF96) according to previous protocol [41]. Ten thousand MEF cells were plated 18 h prior to measurement in complete medium in a 96-well plate. Cells were equilibrated in media containing DMEM lacking bicarbonate (Sigma D5030) 1 h prior to experiment. Oxygen and pH levels were measured over 5-min periods at basal state, and after sequential addition of 2  $\mu\text{M}$  oligomycin, 10  $\mu\text{M}$  CCCP, and 2  $\mu\text{M}$  antimycin A to evaluate maximal mitochondrial respiration. Data are normalized to total protein level in each well.

## Chemical reagents and antibodies

Antimycin A (Santa Cruz), oligomycin (Santa Cruz), CCCP (Sigma), bafilomycin A1 (Sigma), and MitoTracker CMXRos (ThermoFisher) were resuspended in DMSO (Sigma). Antimycin A and oligomycin were stored in aliquots at  $-80^{\circ}\text{C}$ . CCCP and bafilomycin A1 were stored in aliquots at  $-20^{\circ}\text{C}$ . Primary antibodies for immunofluorescent staining include the following: rabbit anti-LC3 (Sigma L7543, 1:5,000), rabbit anti-TOMM20 (Santa Cruz sc-11415, 1:1,000), mouse anti-Parkin (Cell Signaling 4211, 1:1,000), mouse anti-DNA (Millipore CBL186, 1:1,000), mouse anti-ATP5B (Santa Cruz sc-166462, 1:1,000), mouse anti-PEX13 (Santa Cruz sc-271477, 1:100), rabbit anti-PMP70 (Thermo Scientific PA1-650, 1:1,000), mouse anti-Flag (Sigma 184-200UG, 1:1,000), and rabbit anti-WIP1 (Abcam ab105459, 1:500). Secondary antibodies were conjugated to AlexaFluor488, AlexaFluor594, and/or AlexaFluor647 (Invitrogen, 1:750). Primary antibodies for Western blot analyses include the following: mouse anti-PEX13 (Santa Cruz sc-271477, 1:200), rabbit anti-ATG7 (Sigma A2856, 1:1,000), rabbit anti-FANCC (Fanconi Anemia Research Fund FANCC-C2, 1:1,000), mouse anti-SMURF1 (Sigma WH0057154M1, 1:1,000), guinea pig anti-p62 (Progen GP62-C, 1:1,000), rabbit anti-LC3 (Novus NB100-2220, 1:1,000), and HRP-conjugated mouse anti-actin (Santa Cruz sc-47778-HRP, 1:2,000).

## Constructs

The pCMV6 vector expressing human PEX13-MYC-DDK was purchased from Origene. *PEX13* disease-associated mutants I326T and W313G, siRNA-resistant constructs, and constructs without MYC-DDK tags were generated using QuikChange II Site-Directed Mutagenesis kit (Agilent Technologies). *PEX13* constructs with resistance to siPEX13 oligo #2 were generated using two successive steps. Primers are listed in Appendix Table S3.

## Retroviruses and lentiviruses

pMXs-IP-HA-Parkin [20] (Addgene #38248) was cotransfected with the helper plasmids pUMVC and pCMV-VSV-G [42] (Addgene #8849 and #8454) into HEK293T cells. *PEX13* cDNAs containing WT, W313G mutation, and I326T mutation were cloned into pLenti-C-Myc-DDK-IRES-Neo vector (Origene), then cotransfected into HEK293 cells with the helper plasmids pCMV $\Delta$ R8.91 [43] and pMDG [44]. Retro- or lentiviral supernatant was filtered through a 0.45- $\mu\text{m}$  membrane and then added to target cells in the presence of polybrene (8  $\mu\text{g}/\text{ml}$ ). Cells were selected in media containing 0.5  $\mu\text{g}/\text{ml}$  puromycin or 500  $\mu\text{g}/\text{ml}$  G418 and then maintained in media containing 0.25  $\mu\text{g}/\text{ml}$  puromycin and/or 100  $\mu\text{g}/\text{ml}$  G418.

## Statistical analyses

Two-tailed unpaired Student's *t*-test was used for the comparison of means of two normally distributed datasets. ANOVA with adjustment for multiple comparisons was used for comparing multiple conditions to a single control. Kruskal–Wallis *H*-test was used for comparing multiple non-normally distributed datasets to one control. Unless otherwise specified, data shown represent mean  $\pm$  error bars for technical replicates and similar results were observed in at least three independent experiments. Since the absolute values in readouts

of control samples can vary significantly across independent experiments, it is more meaningful to compare experimental conditions to the control conditions within a given experiment.

**Expanded View** for this article is available online.

## Acknowledgements

This work was supported by NIH grants RO1 CA109618 (B.L.), U19 AI109725 (B.L.), and KO8 AI099150 (R.S.); Cancer Prevention Research Institute of Texas (CPRIT) grant RP120718 (B.L.); and a Burroughs Wellcome Career Medical Scientist Award (R.S.). We gratefully acknowledge Suresh Subramani (UC San Diego School of Medicine) for helpful discussions; Noboru Mizushima (University of Tokyo Medical School) for providing critical reagents; Haley Smith for assistance with manuscript preparation; and Lori Nguyen for technical assistance.

## Author contributions

MYL, DIC, HR, and BL designed research; MYL, ZZ, RS, SS, YW, and PM performed research; MYL, PM, and BL analyzed data; and MYL, DIC, and BL wrote the paper.

## Conflict of interest

The authors declare that they have no conflict of interest.

## References

- Wanders RJ (2004) Metabolic and molecular basis of peroxisomal disorders: a review. *Am J Med Genet A* 126A: 355–375
- Fujiki Y, Okumoto K, Mukai S, Honsho M, Tamura S (2014) Peroxisome biogenesis in mammalian cells. *Front Physiol* 5: 307
- Zhang J, Kim J, Alexander A, Cai S, Tripathi DN, Dere R, Tee AR, Tait-Mulder J, Di Nardo A, Han JM et al (2013) A tuberosus sclerosis complex signalling node at the peroxisome regulates mTORC1 and autophagy in response to ROS. *Nat Cell Biol* 15: 1186–1196
- Dixit E, Boulant S, Zhang Y, Lee AS, Odendall C, Shum B, Hacohen N, Chen ZJ, Whelan SP, Fransen M et al (2010) Peroxisomes are signaling platforms for antiviral innate immunity. *Cell* 141: 668–681
- Gould SJ, Kalish JE, Morrell JC, Bjorkman J, Urquhart AJ, Crane DI (1996) Pex13p is an SH3 protein of the peroxisome membrane and a docking factor for the predominantly cytoplasmic PTs1 receptor. *J Cell Biol* 135: 85–95
- Liu Y, Bjorkman J, Urquhart A, Wanders RJ, Crane DI, Gould SJ (1999) PEX13 is mutated in complementation group 13 of the peroxisome-biogenesis disorders. *Am J Hum Genet* 65: 621–634
- Wanders RJ, Waterham HR (2006) Biochemistry of mammalian peroxisomes revisited. *Annu Rev Biochem* 75: 295–332
- Wanders RJ, Waterham HR (2005) Peroxisomal disorders I: biochemistry and genetics of peroxisome biogenesis disorders. *Clin Genet* 67: 107–133
- Zeharia A, Eberink MS, Wanders RJ, Waterham HR, Gutman A, Nissenkorn A, Korman SH (2007) A novel PEX12 mutation identified as the cause of a peroxisomal biogenesis disorder with mild clinical phenotype, mild biochemical abnormalities in fibroblasts and a mosaic catalase immunofluorescence pattern, even at 40 degrees C. *J Hum Genet* 52: 599–606
- Rosewich H, Waterham HR, Wanders RJ, Ferdinandusse S, Henneke M, Hunneman D, Gartner J (2006) Pitfall in metabolic screening in a patient with fatal peroxisomal beta-oxidation defect. *Neuropediatrics* 37: 95–98
- Levine B, Kroemer G (2008) Autophagy in the pathogenesis of disease. *Cell* 132: 27–42

12. Boya P, Reggiori F, Codogno P (2013) Emerging regulation and functions of autophagy. *Nat Cell Biol* 15: 713–720
13. Stolz A, Ernst A, Dikic I (2014) Cargo recognition and trafficking in selective autophagy. *Nat Cell Biol* 16: 495–501
14. Rogov V, Dotsch V, Johansen T, Kirkin V (2014) Interactions between autophagy receptors and ubiquitin-like proteins form the molecular basis for selective autophagy. *Mol Cell* 53: 167–178
15. Choi AM, Ryter SW, Levine B (2013) Autophagy in human health and disease. *N Engl J Med* 368: 1845–1846
16. Orvedahl A, Sumpter R Jr, Xiao G, Ng A, Zou Z, Tang Y, Narimatsu M, Gilpin C, Sun Q, Roth M et al (2011) Image-based genome-wide siRNA screen identifies selective autophagy factors. *Nature* 480: 113–117
17. Orvedahl A, MacPherson S, Sumpter R Jr, Talloczy Z, Zou Z, Levine B (2010) Autophagy protects against Sindbis virus infection of the central nervous system. *Cell Host Microbe* 7: 115–127
18. Sumpter R Jr, Sirasanagandla S, Fernandez AF, Wei Y, Dong X, Franco L, Zou Z, Marchal C, Lee MY, Clapp DW et al (2016) Fanconi anemia proteins function in mitophagy and immunity. *Cell* 165: 867–881
19. Padman BS, Bach M, Lucarelli G, Prescott M, Ramm G (2013) The protonophore CCCP interferes with lysosomal degradation of autophagic cargo in yeast and mammalian cells. *Autophagy* 9: 1862–1875
20. Yoshii SR, Kishi C, Ishihara N, Mizushima N (2011) Parkin mediates proteasome-dependent protein degradation and rupture of the outer mitochondrial membrane. *J Biol Chem* 286: 19630–19640
21. Maxwell M, Bjorkman J, Nguyen T, Sharp P, Finnie J, Paterson C, Tonks I, Paton BC, Kay GF, Crane DI (2003) Pex13 inactivation in the mouse disrupts peroxisome biogenesis and leads to a Zellweger syndrome phenotype. *Mol Cell Biol* 23: 5947–5957
22. Shimozawa N, Suzuki Y, Zhang Z, Imamura A, Toyama R, Mukai S, Fujiki Y, Tsukamoto T, Osumi T, Orii T et al (1999) Nonsense and temperature-sensitive mutations in PEX13 are the cause of complementation group H of peroxisome biogenesis disorders. *Hum Mol Genet* 8: 1077–1083
23. Krause C, Rosewich H, Woehler A, Gartner J (2013) Functional analysis of PEX13 mutation in a Zellweger syndrome spectrum patient reveals novel homooligomerization of PEX13 and its role in human peroxisome biogenesis. *Hum Mol Genet* 22: 3844–3857
24. Polson HE, de Lartique J, Rigden DJ, Reedijk M, Urbe S, Claque MJ, Tooze SA (2010) Mammalian Atg18 (WIPI2) localizes to omegasome-anchored phagophores and positively regulates LC3 lipidation. *Autophagy* 6: 506–522
25. Huybrechts SJ, Van Veldhoven PP, Brees C, Mannaerts GP, Los GV, Franssen M (2009) Peroxisome dynamics in cultured mammalian cells. *Traffic* 10: 1722–1733
26. Burnett SF, Farre JC, Nazarko TY, Subramani S (2015) Peroxisomal Pex3 activates selective autophagy of peroxisomes via interaction with the pexophagy receptor Atg30. *J Biol Chem* 290: 8623–8631
27. Yamashita S, Abe K, Tatemichi Y, Fujiki Y (2014) The membrane peroxin PEX3 induces peroxisome-ubiquitination-linked pexophagy. *Autophagy* 10: 1549–1564
28. Kirkin V, McEwan DG, Novak I, Dikic I (2009) A role for ubiquitin in selective autophagy. *Mol Cell* 34: 259–269
29. Wild P, Farhan H, McEwan DG, Wagner S, Rogov VV, Brady NR, Richter B, Korac J, Waidmann O, Choudhary C et al (2011) Phosphorylation of the autophagy receptor optineurin restricts Salmonella growth. *Science* 333: 228–233
30. Matsumoto G, Wada K, Okuno M, Kurosawa M, Nukina N (2011) Serine 403 phosphorylation of p62/SQSTM1 regulates selective autophagic clearance of ubiquitinated proteins. *Mol Cell* 44: 279–289
31. Baumgart E, Vanhorebeek I, Grabenbauer M, Borgers M, Declercq PE, Fahimi HD, Baes M (2001) Mitochondrial alterations caused by defective peroxisomal biogenesis in a mouse model for Zellweger syndrome (PEX3 knockout mouse). *Am J Pathol* 159: 1477–1494
32. Salpietro V et al (2015) Zellweger syndrome and secondary mitochondrial myopathy. *Eur J Pediatr* 174: 557–563
33. Ding WX, Yin XM (2012) Mitophagy: mechanisms, pathophysiological roles, and analysis. *Biol Chem* 393: 547–564
34. Li ML, Wang HL, Stollar V (1997) Complementation of and interference with Sindbis virus replication by full-length and deleted forms of the nonstructural protein, nsP1, expressed in stable transfectants of HeLa cells. *Virology* 227: 361–369
35. Su T, Suzui M, Wang L, Lin CS, Xing WQ, Weinstein IB (2003) Deletion of histidine triad nucleotide-binding protein 1/PKC-interacting protein in mice enhances cell growth and carcinogenesis. *Proc Natl Acad Sci USA* 100: 7824–7829
36. Mizushima N, Yamamoto A, Matsui M, Yoshimori T, Ohsumi Y (2004) In vivo analysis of autophagy in response to nutrient starvation using transgenic mice expressing a fluorescent autophagosome marker. *Mol Biol Cell* 15: 1101–1111
37. Liang XH, Kleeman LK, Jiang HH, Gordon G, Goldman JE, Berry G, Herman B, Levine B (1998) Protection against fatal Sindbis virus encephalitis by Beclin, a novel Bcl-2-interacting protein. *J Virol* 72: 8586–8596
38. Hardwick JM, Levine B (2000) Sindbis virus vector system for functional analysis of apoptosis regulators. *Methods Enzymol* 322: 492–508
39. Shoji-Kawata S, Sumpter R, Leveno M, Campbell GR, Zou Z, Kinch L, Wilkins AD, Sun Q, Pallauf K, MacDuff D et al (2013) Identification of a candidate therapeutic autophagy-inducing peptide. *Nature* 494: 201–206
40. Liang XH, Jackson S, Seaman M, Brown K, Kempkes B, Hibshoosh H, Levine B (1999) Induction of autophagy and inhibition of tumorigenesis by beclin 1. *Nature* 402: 672–676
41. Mishra P, Carelli V, Manfredi G, Chan DC (2014) Proteolytic cleavage of Opa1 stimulates mitochondrial inner membrane fusion and couples fusion to oxidative phosphorylation. *Cell Metab* 19: 630–641
42. Stewart SA, Dykxhoorn DM, Palliser D, Mizuno H, Yu EY, An DS, Sabatini DM, Chen IS, Hahn WC, Sharp PA et al (2003) Lentivirus-delivered stable gene silencing by RNAi in primary cells. *RNA* 9: 493–501
43. Zufferey R, Nagy D, Mandel RJ, Naldini L, Trono D (1997) Multiply attenuated lentiviral vector achieves efficient gene delivery in vivo. *Nat Biotechnol* 15: 871–875
44. Naldini L, Blomer U, Gally P, Ory D, Mulligan R, Gage FH, Verma IM, Trono D (1996) In vivo gene delivery and stable transduction of nondividing cells by a lentiviral vector. *Science* 272: 263–267



**License:** This is an open access article under the terms of the Creative Commons Attribution-NonCommercial-NoDerivs 4.0 License, which permits use and distribution in any medium, provided the original work is properly cited, the use is non-commercial and no modifications or adaptations are made.